

# Experimental studies of mercury molecules

R. E. Drullinger, M. M. Hessel, and E. W. Smith

Laser Physics Section, National Bureau of Standards, Boulder, Colorado 80302  
(Received 10 January 1977)

Optically excited fluorescence spectra in pure mercury vapor have been studied over the spectral range 240–600 nm for temperatures between 400–1000 K and densities between  $5 \times 10^{16}$ – $2 \times 10^{19}$   $\text{cm}^{-3}$ . Absorption measurements were made over the spectral range 253–334 nm, and both structured and continuum bands were observed. Several types of two photon experiments were also performed in order to probe the excited states of the mercury dimer. In addition, the mercury spectrum from mercury vapor–noble gas mixtures has also been studied for noble gas pressures up to 1 atm.

## I. INTRODUCTION

In the present paper we discuss extensive spectroscopic measurements on mercury vapor. We have used absorption, fluorescence, and two photon techniques in order to provide a large body of data for analysis of the molecular species encountered in mercury vapor at pressures ranging from 1 torr (133.3 Pa) to 4 atm ( $4 \times 10^5$  Pa), which is the pressure range of interest in mercury excimer laser research. Our analysis of these data is presented in the following paper.<sup>(1)</sup>

Broad band molecular fluorescence from optically excited mercury vapor was studied in the early 1900's by Wood<sup>2</sup> and co-workers and by Lord Rayleigh<sup>3</sup> who excited the mercury vapor using the 253.7 nm  $6^1S_0$ – $6^3P_1$  mercury resonance line. Since that time, several attempts have been made to study the molecular structure of the molecules emitting these bands using both optical<sup>4–9</sup> and electrical<sup>10–14</sup> excitation schemes. The results obtained by electrical excitation are complicated by the presence of charged particles and very highly excited atoms and molecules that can emit or absorb radiation and thereby alter the observed spectra in a complicated manner. Furthermore, the spectra observed with electrical excitation often differ quite radically from those obtained by optical pumping. In this paper we will consider only optically excited spectra since we feel this is a much cleaner method for studying the molecular structure of the radiating species. Once the molecular structure is understood, one can proceed to study the properties of electrical discharges (e.g., Mosburg and Wilke).<sup>15</sup>

We have measured the fluorescence spectrum of pure mercury from 240 to 600 nm with a resolution of 2 nm for a number of temperatures between 400 and 1000 K and densities between  $5 \times 10^{16}$  and  $2.2 \times 10^{19}$   $\text{cm}^{-3}$ . These spectra were taken in order to permit a detailed analysis of the potential curves for the radiative transitions. Owing to the large amount of data collected, an automated measurement system was developed. These fluorescence measurements are discussed in Sec. II. Fluorescence measurements at higher resolution showed the presence of vibrational bands for some spectral regions; these are discussed in Sec. V.

Absorption measurements have been made from 253 to 334 nm, and both structured and continuous spectra were observed. Absolute absorption measurements were made at a few wavelengths, and their temperature

and density dependence were analyzed in order to obtain the *A* values for the transitions as well as the energy levels of the states involved. These measurements are discussed in Sec. III.

Finally, two photon measurements were made in order to probe the excited states of the mercury dimer. A 257.2 nm pump laser was used to excite the vapor and various probe lasers were used together with synchronous detection of the fluorescence in order to distinguish excited state absorption and emission. These measurements are discussed in Sec. IV.

## II. FLUORESCENCE MEASUREMENTS

### A. Containment cells

Mercury is known to react with many atomic and molecular species,<sup>(16)</sup> and the spectra of impurity compounds are sometimes incorrectly identified as  $\text{Hg}_2$ .<sup>17</sup> Furthermore, oxygen and some other foreign gases<sup>16,2</sup> are very effective at quenching excited mercury atoms. It was thus necessary to take great pains to insure chemical purity of the mercury and the containment cells used in our experiments. In Sec. (2. B) of Ref. 6, we describe a distillation process that we use to fill our sample cells with pure mercury. The sample cells themselves were made from quartz tubing with uv grade quartz windows either fused or optically contacted to the cell body. The cells had a small tube extending downward from the main cell body that served as a reservoir for the liquid mercury. The cells were contained in a two compartment oven, constructed of low density fire brick, in which the compartments were heated separately. The upper part of the oven, which contained the main cell body, determined the mercury vapor temperature and was always hotter than the lower oven. The lower oven controlled the temperature of the mercury reservoir tube (i.e., cold finger) and thus determined the vapor density in the cell. With this arrangement, it was possible to independently vary the temperature and density in the main cell body. Cells of this design were operated at mercury pressures up to 4 atm.

The temperature in the upper and lower ovens were independently regulated and could be held constant to within a few hundredths of a degree. This was necessary since a temperature fluctuation of 0.1 K in the lower oven could produce a density variation the order of 0.2% that would have produced observable errors in some spectral measurements (e.g., the intensity of the

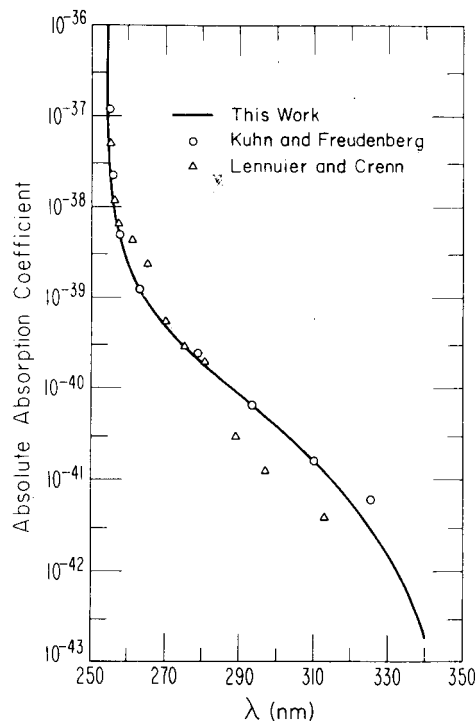


FIG. 1. Absorption coefficient  $k(\lambda, T) = -\ln[I(\lambda, T)/I_0(\lambda)]/n^2x$  where  $n^2$  is the mercury density in  $\text{cm}^{-3}$  and  $x$  denotes the optical path length in cm. Our data were measured at 773 K whereas those of Kuhn and Freudenberg<sup>5</sup> were measured at 1073 K and those of Lennuier and Crenn<sup>7</sup> at 650 K. This results in a slight deviation for  $\lambda > 280$  nm owing to the fact that the  $\text{Hg}_2$  ground state becomes increasingly repulsive at the internuclear separations responsible for these wavelengths.

485 band is proportional to the cube of the density in some cases). The upper oven also had to be temperature controlled to 0.5 K since the relative intensity of the observed fluorescence bands varied exponentially with temperature.

### B. Optical excitation schemes

The most common method of exciting mercury vapor is to use the 253.7 nm resonance line from a mercury lamp. The  $A$  value for this line<sup>18</sup> is the order of  $10^7 \text{ sec}^{-1}$ ; thus at densities greater than  $10^{16} \text{ cm}^{-3}$  all of the exciting radiation is absorbed in a thin sheath at the wall of the cell. Resonance line excitation is thus restricted to rather low mercury pressures, and it is often necessary to add a catalyst such as  $\text{N}_2$  to the vapor in order to form mercury molecules. It is desirable however to use pure mercury at higher pressures where the analysis of the data is simplified by the fact that many states come into thermal equilibrium.<sup>1</sup>

In order to optically excite the vapor at higher pressures it is desirable to pump in the wings of the 253.7 nm line where the absorption cross section and the optical depth are lower. Lennuier and Crenn<sup>7</sup> and Kuhn and Freudenberg<sup>5</sup> have shown that the 253.7 nm line has a very broad red wing that absorbs radiation from line center out to 320 nm and beyond. Figure 1 shows our measurement of this wing absorption from 254–334 nm. Here we have defined the absorption coeffi-

cient as  $k = -\ln(I/I_0)/n^2x$ , where  $n$  is the mercury density in  $\text{cm}^{-3}$  and  $x$  is the absorption path length in cm. Plotted on top of our curve is the relative absorption data of Kuhn and Freudenberg normalized to our data at 263 nm. Also on this figure are the data of Lennuier and Crenn that represent the 335 nm band fluorescence intensity as a function of exciting wavelength at a pressure of  $8 \times 10^4 \text{ Pa}$  (600 torr). These data are normalized to ours at 275 nm.

Several types of broad band continuum lamps<sup>16,19</sup> have been used to excite mercury vapor via this absorption. Such lamps can provide volume excitation, and we used this method extensively in our early work on mercury vapor.<sup>6</sup> However, the broad band radiation from the lamp is scattered by the mercury vapor, and this scattered signal can mask some of the features of interest in the blue wing of the 335 nm molecular band. We have found that it is possible to obtain much higher pump power densities with less problem from scattered pump radiation by using the frequency doubled radiation from the 514.5 nm argon ion laser line. Using a commercial 10 W argon ion laser and an ADP crystal doubler we obtained a 2 mm diam 15 mW laser beam at 257.2 nm.

### C. Detection system

Most of the data were taken with the apparatus shown in Fig. 2. The spectra were scanned with a  $\frac{1}{3}$  m spectrometer from 240 to 650 nm with a 2 nm resolution. The detector was a cooled phototube with an S-20 response. This detection system was calibrated using a standard lamp, and all data reported are proportional to the number of photons emitted per unit wavelength. The pump laser was chopped, and synchronous detection of the fluorescence was used to avoid the strong blackbody radiation from the oven. The output signal was fed into a 1024 channel multichannel analyser (MCA). The spectrometer grating was advanced in 0.01 nm steps by a stepping motor, and the MCA channel number was advanced every 20 steps. In order to remove the effect of power variations in the pump laser, a separate feedback system was employed (see Fig. 2). This system consisted of a phototube which observed the 335 nm band fluorescence through a filter. When the integrated signal observed by this detector reached a predetermined level, a pulse was sent to the grating stepping motor. Thus, if the laser power should drift to a lower level, the molecular fluorescence would decrease and the length of that time interval would be correspondingly increased to remove the effect of this fluctuation. The output from the MCA was stored on a magnetic tape. After several runs at different temperatures and densities the tape recorded data were analyzed by computer programs that applied the system calibration function, made microfilm plots of the calibrated data, and stored it on disks for the theoretical analysis discussed by Smith *et al.*<sup>11</sup>

When scanning wavelengths longer than 445 nm, a filter giving a  $10^4$  times attenuation for  $\lambda < 340$  nm was inserted in the optical path. This was done to remove second order spectra resulting from the strong molec-

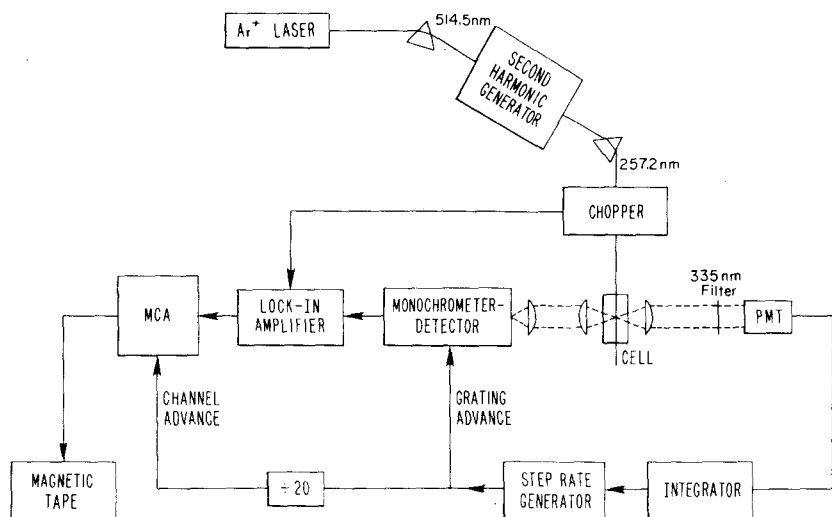


FIG. 2. Schematic diagram of the apparatus used for fluorescence measurements.

ular fluorescence in the 335 nm band. The transmission function for this filter was measured, and it was accounted for in the computer program which calibrated the spectral data.

#### D. Temperature and density dependence of fluorescence bands

Some of the first measurements made were scans of the band shapes as functions of temperature and density [Figs. 3-6]. It is interesting to note that the peak of the 485 band occurs closer to 500 nm than to 485 nm. In our uncalibrated traces the peak occurred at 485 nm, but when the data are corrected for the rapid decrease in spectrometer phototube response at red wavelengths, the true peak appears at 500 nm. The 335 band shape

is essentially unaffected by the calibration. Since the true band shapes and the location of the point of maximum intensity are very important quantities in the analysis of the spectral data, it is essential to use a well calibrated detection system.

From Figs. 3 and 4 it is clear that neither band shape is affected by density changes. However, the band shapes are strongly affected by changes in temperature, Figs. 5 and 6. In these figures, the integrated band intensities are normalized to unity to show the shifts of the populations within the respective bands. As temperature is increased both bands show a decrease in peak intensity, an overall broadening of the band, and a slight shift toward the blue. This is consistent with a thermal (Boltzmann) distribution of vibrational states (this pop-

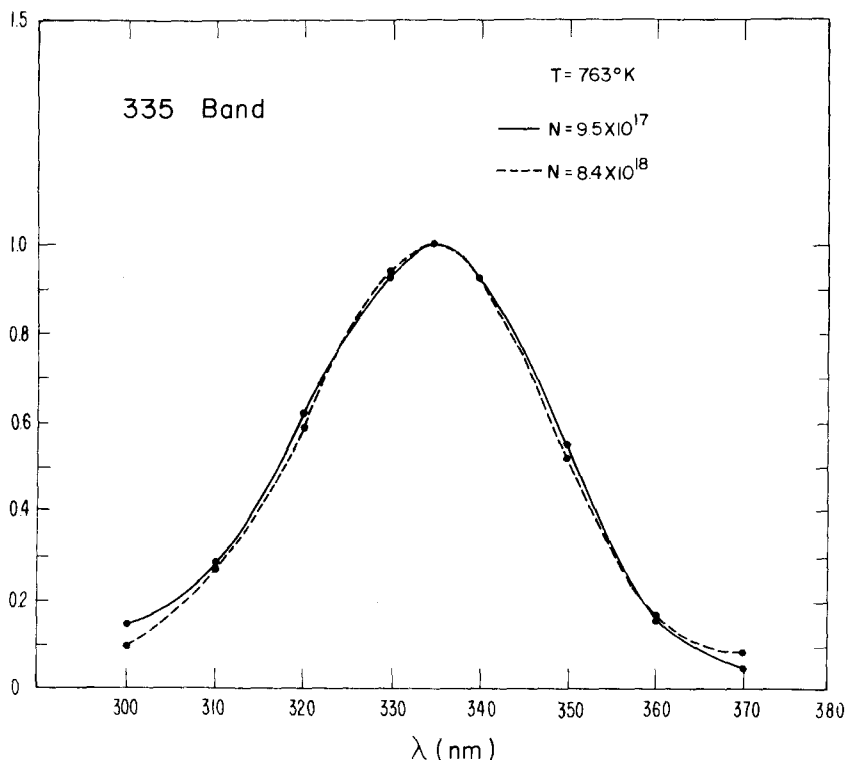


FIG. 3. 335 band shape as a function of density (in  $\text{cm}^{-3}$ ) at a fixed temperature of 763 K.

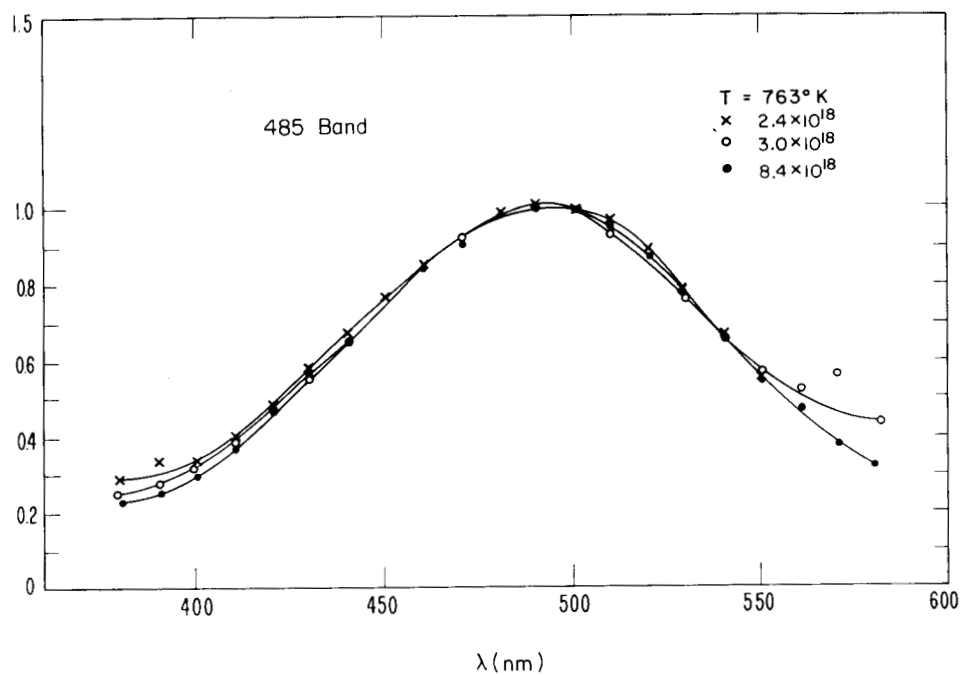


FIG. 4. 485 band shape as a function of density (in  $\text{cm}^{-3}$ ) at a fixed temperature of 763 K.

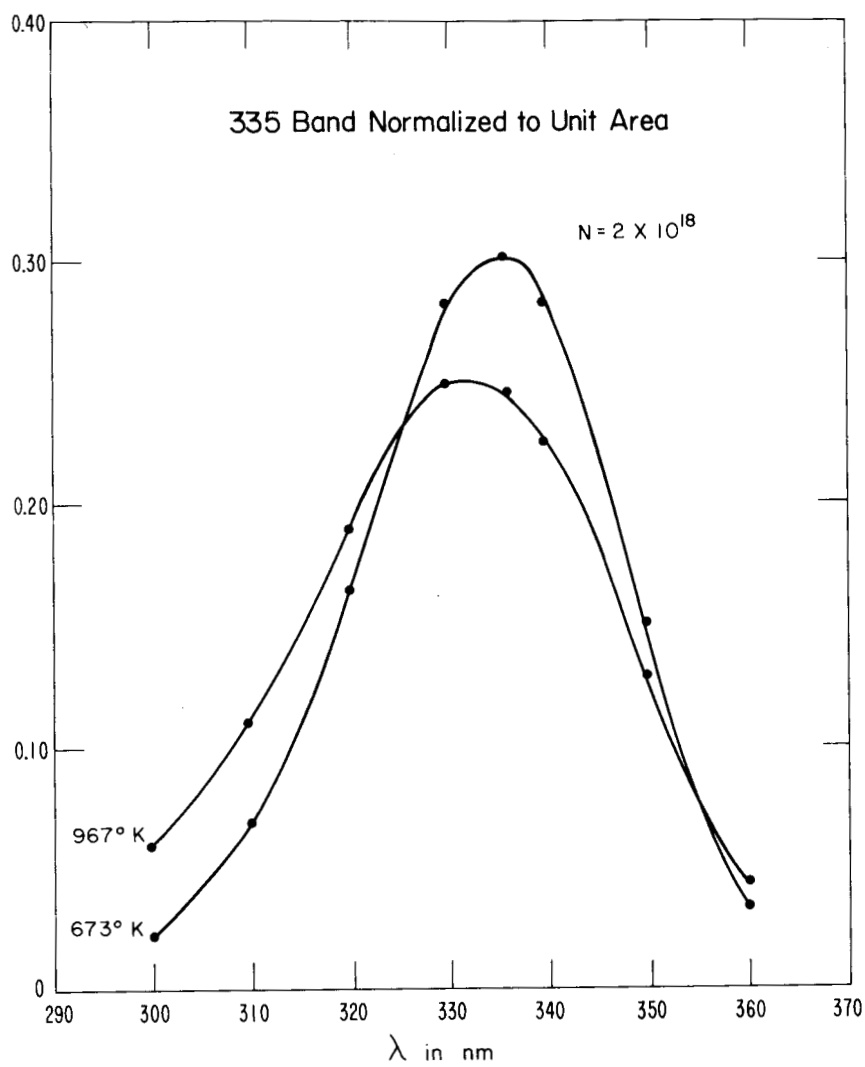


FIG. 5. 335 band shape as a function of temperature at a fixed density of  $2 \times 10^{18} \text{cm}^{-3}$ . Both curves are normalized to unit area to show the effect of the shift of population within the radiating state.

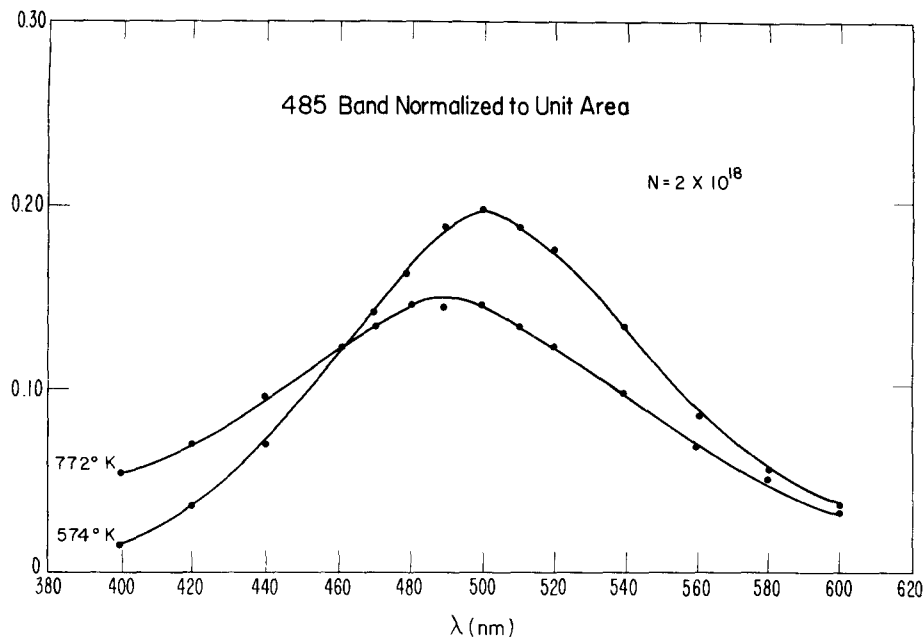


FIG. 6. 485 band shape as a function of temperature at a fixed density of  $2 \times 10^{18} \text{ cm}^{-3}$ . Both curves are normalized to unit area to show the effect of the shift of population within the radiating state.

ulation distribution is verified by a detailed analysis presented in Sec. II of Ref. 1); that is, an increase in temperature shifts population from the bottom of the well, which radiates the maximum intensity, to higher lying states, which emit in the wings of the band. The precise location of the peak emission intensity is determined by a product of the population and the transition probability. Since the latter increases with decreasing wavelength (Ref. 1), the actual emission peak is slightly blue shifted relative to where it would be for a wavelength independent transition probability. As the temperature is increased and the population thereby shifted to higher vibrational states, the emission maximum is thus shifted more to the blue. This broadening and shift of the emission maximum with increasing temperature has been used very effectively by Mosburg and Wilke<sup>15</sup> to determine the vibrational temperature of mercury molecules in an electrical discharge.

The next measurements to be made were the density and temperature dependence of the ratio of integrated 335 and 485 nm band intensities. The results of several such measurements are shown in Fig. 4 of Ref. 1. After careful calibration and least squares fitting of the data, it was found that all of the data for mercury atom densities greater than  $3 \times 10^{17} \text{ cm}^{-3}$  and gas temperature greater than 575 K could be described by a function of the form.

$$I_{485}/I_{335} = 2.2 \times 10^{-24} n \exp(6500/kT), \quad (2.1)$$

where  $kT$  is given in  $\text{cm}^{-1}$  and the mercury atom density  $n$  is in  $\text{cm}^{-3}$ . These results indicate that the two electronic states responsible for the 485 and 335 bands are in thermal equilibrium (see Sec. II of Ref. 1 for further discussion) for this range of densities and temperatures. They also show that the two bands do not arise from the same molecular species. Since the 335 nm band is known to arise from a mercury dimer (owing to its  $n^2$  density dependence in absorption discussed in Sec. III),

the 485 nm band must then come from some form of triatomic species. This triatomic molecule could be either a stable  $\text{Hg}_3$  molecule or a collision complex in which an  $\text{Hg}_2$  molecule in a metastable state is induced to radiate during a collision with an atom. In the latter case the interaction between the atom and the molecule breaks the symmetries that forbid radiation. In general one would expect this interaction to be a dispersion interaction which is not unique to mercury atoms as perturbers. Thus it should be possible to determine which mechanism produces the 485 band by making the dominant collision partner something other than a mercury atom. A set of such experiments is discussed in the following section.

#### E. Effect of foreign gases on the mercury system

In order to distinguish between the collision induced versus the bound  $\text{Hg}_3$  models for the 485 nm band emission, discussed in the previous section, a series of experiments were performed in which various gases were mixed with the mercury vapor. To simplify the interpretation of the results from these experiments, the mercury density was maintained at  $3 \times 10^{17} \text{ cm}^{-3}$ . In this way the mercury density itself was sufficient to maintain thermal equilibrium between the states radiating 335 nm and 485 nm (see previous section) but low enough to allow the foreign gas perturber to be the dominant collision partner (by as much as 100 $\times$ ). The cell and oven were similar in construction to that described in Sec. IIB but the bakeout and filling procedures had to be modified. The cell was connected to a high vacuum system through a stainless steel valve which was kept at a temperature above that of the reservoir. The gases were all research purity, and the noble gases (He, Ar, Kr, Xe) were maintained clean with a barium getter whereas, the  $\text{N}_2$  was cleaned with a magnesium getter.

During any given experimental run the cell was evac-

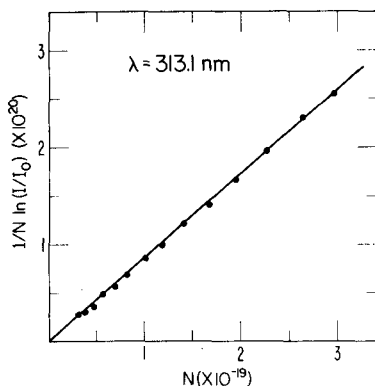


FIG. 7. 313.1 nm absorption coefficient  $\ln[I(\lambda, T)/I_0(\lambda)]$  divided by the mercury atom density  $N$  in  $\text{cm}^{-3}$ . The linear density dependence of this function and its zero intercept show that the absorption coefficient is a function only of  $N^2$  (i.e., molecular absorption).

uated, the Hg density brought up to  $3 \times 10^{17} \text{ cm}^{-3}$ , a spectrum of the excimer fluorescence was recorded, the buffer gas density was brought up in steps while the ratio of the band intensities was monitored and, at the highest gas density, the excimer fluorescence spectrum was again recorded. With each of the gases used, there was no change in the relative band intensities or in the spectral content of the excimer fluorescence except for a transient during the diffusional mixing of the buffer gas with the mercury vapor. This would indicate the pressure dependent process by which the 485 nm radiator is generated is mercury specific. Such a specificity would not be expected in a collision induced radiation process.

### III. ABSORPTION MEASUREMENTS

#### A. Apparatus

The absorption measurements were made in a cylindrical quartz cell 70.9 cm in length which was filled by the distillation procedure outlined in Sec. II. Again a cold finger was used to fix the density in the cell and the temperature of the cell was maintained by a separate heater so that temperature and density could be varied independently. The temperature in the absorption cell was constant to within 1% over the absorption path and the density could be held constant to within 1%.

Measurements were attempted using a broad band Xe light source filtered by a premonochromator. It was found that the signal to noise ratio was very small with this method. To improve the signal to noise ratio, the intense spectral lines emitted by a medium pressure mercury lamp were used. With this source it was possible to use very narrow band detection resulting in a great improvement in the signal to noise ratio.

The absorption of the empty cell (i.e., zero mercury density) was measured in order to correct for losses in the end windows; the latter was found to have a slight temperature dependence for most wavelengths, perhaps due to a slight bending of the rather long absorption cell. It was also found that changes in the cold finger

temperature (i.e., pressure changes) took over 1 h to equilibrate throughout the cell; thus it was necessary to wait a few hours between runs to insure that the cell had come to equilibrium before each measurement.

After the cell had been suitably calibrated, absorption measurements were made at the wavelengths 257.6, 265.2, 280, 296.7, 313.1, and 334.1 nm using the medium pressure mercury lamp. Additional measurements were made at 298 nm with a Cd line source and at 257.2 nm with the frequency doubled argon laser line.

#### B. Analysis of data

The absorption of radiation of wavelength  $\lambda$  in an absorption path of length  $L$  is described by

$$I(\lambda, L) = I_0(\lambda) \exp[-k(\lambda)L] \quad (3.1)$$

For bound-free transitions in a diatomic molecule, the absorption coefficient is given by [Eq. (2.5) of Ref. 1]

$$k(\lambda) = n^2 k_m(\lambda, T) = n^2 k_1(\lambda) \exp[-V(\lambda)/kT], \quad (3.2)$$

where  $n$  is the ground state atom density,  $T$  is the gas temperature, and  $V(\lambda)$  is the ground state energy at which the radiative transition takes place (according to the Frank-Condon principle). The coefficient  $k_1(\lambda)$  contains the  $A$  value for the radiative transition, a line shape function and various constants that are all independent of temperature and density. The general procedure in the absorption measurements is to plot the log of  $I(\lambda, L)/I_0(\lambda)$  versus  $1/kT$  for a fixed  $n$ . The slope of this plot will then give  $V(\lambda)$ , and the infinite temperature intercept will give  $n^2 k_1(\lambda)$ . Thus, knowing  $n^2$ , both  $V(\lambda)$  and  $k_1(\lambda)$  can be obtained for several values of  $\lambda$ . As a check on the validity of this procedure, plots were also made of  $(1/n)\ln[I(\lambda, L)/I_0(\lambda)]$  versus  $n$ . Such plots should be linear with a zero intercept at  $n=0$  as in Fig. 7.

However, some plots had a nonzero intercept at  $n=0$ , as in Fig. 8, indicating that the absorption coefficient is described by a function of the form

$$k(\lambda) = n^2 k_m(\lambda, T) + n k_a(\lambda, T) \quad (3.3)$$

After the experiments had been completed, it was discovered that the additional absorption,  $k_a$ , was due to atomic lines originating from the  $6^3P_0$  and  $6^3P_1$  states. Although it is possible to remove the effect of this atomic absorption (as discussed in the Appendix), it

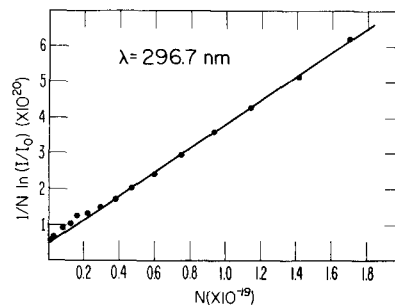


FIG. 8. 296.7 nm absorption coefficient  $\ln[I(\lambda, T)/I_0(\lambda)]$  divided by the mercury atom density  $N$  in  $\text{cm}^{-3}$ . The fact that this function does not extrapolate to zero at zero gas density indicates the presence of additional nonmolecular absorbers.

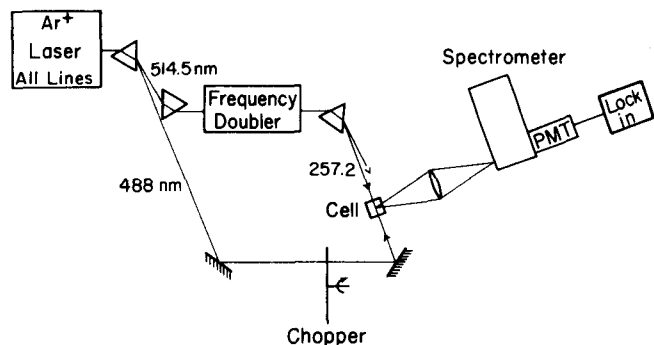


FIG. 9. Schematic diagram of the apparatus used for two photon experiments.

was decided that the data were noisy enough without the added uncertainty resulting from such a correction. Thus only the data at 257.2, 265, 280, 313.1, 334 nm, which had only  $n^2$  dependent absorption coefficients, were used in the final analysis.

For this set of spectral lines, the ground state potential energies and transition  $A$  values were extracted by plotting  $(1/n) \log[I(\lambda, L)/I_0(\lambda)]$  versus  $1/kT$  as discussed above. In this analysis it was found that the molecular absorption coefficient (which was proportional to  $n^2$ ) did not always have a single exponential temperature dependence as was assumed in writing Eq. (3.2). In the two cases where a simple Boltzmann temperature dependence was not found (i. e., 257.2 nm and 265 nm) it was possible to obtain an excellent fit to the data using a sum of two exponentials

$$k_m = n^2 [k_0(\lambda)e^{-E_0/kT} + k_1(\lambda)e^{-E_1/kT}], \quad (3.4)$$

indicating that there were two different transitions absorbing at the same wavelength. These data were interpreted in terms of two transitions from the  $0_g^+$  ground state, the first from low in the  $0_g^+$  curve into the  $1_u$  curve as expected and the second from high on the repulsive wall of the  $0_g^+$  into the  $0_g^+$  curve arising from the  $^3P_1$  asymptote. The latter transition corresponds to the far wing of the 254 nm band (Fig. 12).

In addition to the absorption measurements in the range 257.2–334 nm, there were also several attempts made to find absorption in the vicinity of the 485 nm band. These measurements were made in shorter cells; essentially the same as those used in the fluorescence measurements. A 488 nm argon laser line was used as a light source and, even at pressures in excess of one atmosphere, no absorption was observed nor any laser induced fluorescence in either molecular band.

#### IV. SEQUENTIAL TWO PHOTON EXCITATION

In this paper, sequential two photon excitation refers to the absorption of pump photons in order to produce excited states that are then studied by the absorption of probe photons.

The cells and 257.2 nm laser excitation scheme (pump laser) described in Sec. IIB were used to provide a high steady state excimer density (approximately  $10^{12} \text{ cm}^{-3}$ ) in the manifold of molecular states which arise from the  $6^3P$  atomic states. This excimer population was then probed by a second laser to look for gain on transitions

to the ground state or excited state absorption. Four types of measurements have been made by this method: (1) a 1 W 488 nm argon laser line was used to look for excited state absorption or gain in the 485 nm band, (2) a 10 mW He–Cd laser at 325 nm was used to look for excited state absorption or gain on the 335 nm band, (3) a 1 W NdYAG laser at  $1.06 \mu\text{m}$  was used in an attempt to induce transitions from the  $0_g$  metastable states to the radiating  $1_u$  state (see Fig. 7 of Ref. 1), and finally (4) the 257.2 nm pump laser was focused to  $10^{-2} \text{ cm}^2$  giving a power density the order of  $1.5 \text{ W/cm}^2$  that was enough to induce two photon absorption.

The system employing the 488 nm argon laser line as a probe is shown in Fig. 9. The probe beam was chopped (300 Hz) and focused to  $10^{-2} \text{ cm}^2$  colinearly with the 257.2 nm pump laser. The modulated fluorescence signal was measured with a lock-in detector, and this signal is plotted as the dashed curve in Fig. 10; the solid curve gives the unmodulated fluorescence for comparison. In this figure, a positive signal (downward direction) corresponds to an increase in fluorescence when the probe laser is on and a negative signal corresponds to a decrease in fluorescence intensity due to the probe laser. This modulated signal is shown on an expanded scale in Fig. 11. The probe laser reduced the fluorescence intensity at all wavelengths except 225, 235, 254, and 488 nm. The 488 nm line is due simply to the strong scattered light from the probe laser. Under high resolution, the 235 and 254 nm features prove to be highly structured molecular bands 1 nm wide whereas the 225 nm band is an unstructured band 20 nm wide. A tentative assignment of these transitions is given in Fig. 12 using the qualitative behavior of the

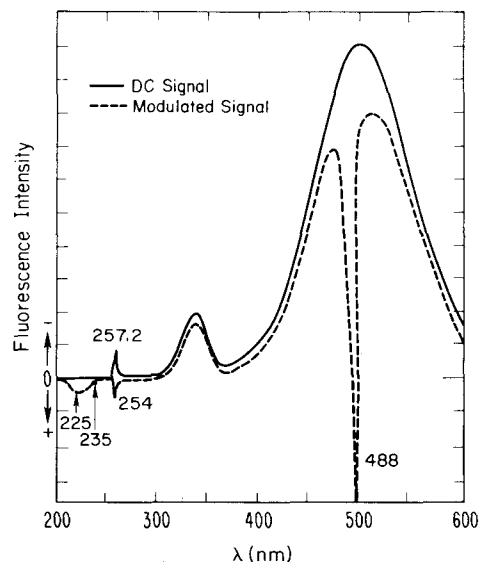


FIG. 10. Fluorescence spectrum observed with two photon pumping using a cw 257.2 nm pump laser and a modulated 488 nm probe laser. The continuous fluorescence (without the probe laser) is shown as a solid line for reference purposes. The synchronously detected two photon fluorescence is represented by the dashed curve. In the latter, a positive signal corresponds to an increase in fluorescence when the probe laser is on and a negative signal corresponds to a decrease in fluorescence intensity due to the probe laser.



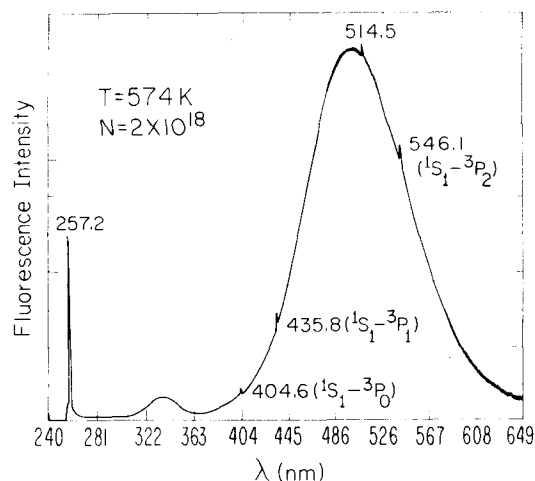


FIG. 13. Two photon induced fluorescence at a density of  $2 \times 10^{18} \text{ cm}^{-3}$  using the 257.2 nm laser as both a probe and a pump laser. The atomic lines at 404.6, 435.8, and 546.1 nm indicate that the  $7^1S_1$  state has been excited by a two photon process, perhaps via molecular absorption into a purely repulsive state that dissociates to a  $7^1S_1 + 6^1S_0$  asymptote. The features at 257.2 and 514.5 nm are due to scattered light from the pump laser and the primary argon laser line which was frequency doubled to produce the pump laser beam.

cence between 265 and 295 nm (see Figs. 14 and 15). The structure terminates to the red of 295 nm because the internuclear separations responsible for wavelength longer than 295 nm correspond to ground state energies above the dissociation energy (e.g., see Table I of Ref. 1). The structure terminates to the blue of 265 nm because the  $1_u$  excited state can predissociate by means of a radiationless transition to the  $0_u^+$  state (see Fig. 17). This structure would indicate a vibrational spacing the order of  $150 \text{ cm}^{-1}$ , but a complete analysis has not been done because natural mercury contains six relatively abundant isotopes which broaden and shift the spectral features.

There is a fluorescence band at 265 nm that can be seen at low densities,  $n < 10^{17}$ , where the higher  $1_u$  vibrational states are out of equilibrium with the lower vibrational states. This band has been seen by Matland and McCoubrey<sup>23</sup> using the 253.7 nm mercury resonance line as an optical pump (see Fig. 16). Their data show that the 265 nm band decreases in intensity relative to the 335 nm band when either density or temper-

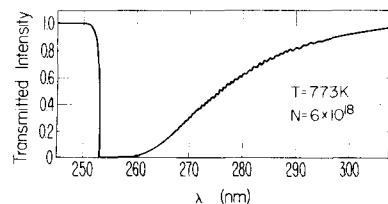


FIG. 14. Transmitted intensity observed with 0.05 nm resolution using a Xe continuum lamp as a light source and a 70.9 cm absorption path at a density of  $6 \times 10^{18} \text{ cm}^{-3}$  and a temperature of 773 K. The structure observed between 265 and 295 nm correspond to those seen in emission, Fig. 15, and indicate a vibrational spacing the order of  $150 \text{ cm}^{-1}$ .

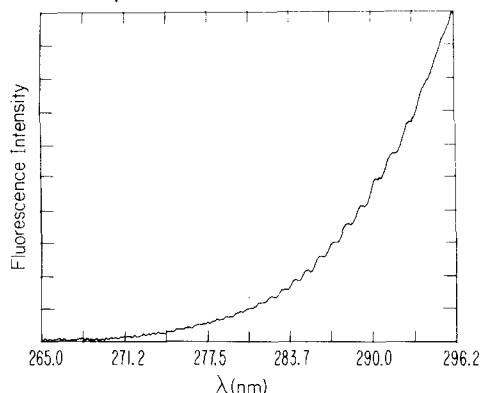


FIG. 15. Fluorescence intensity observed with 0.08 nm resolution from optically excited mercury vapor at a density of  $2 \times 10^{18} \text{ cm}^{-3}$ . The vibrational structure observed correspond to those seen in absorption, Fig. 14, and indicate a vibrational spacing the order of  $150 \text{ cm}^{-1}$ .

ature are increased. We have also seen this band at low temperatures and densities where there is no thermal equilibrium and in pulsed excitation experiments at early times before thermal equilibrium is established. This band arises because the molecular states are populated by three body recombination from the  $6^3P_0$  metastable atomic state (see Fig. 17). Thus when the vibrational thermalization rate does not exceed the radiation rate for the  $1_u$  state (i.e., densities less than  $10^{17} \text{ cm}^{-3}$ ), the vibrational population will have a nonthermal peak at the energy level which is fed by the  $6^3P_0$  atomic state. As shown in Fig. 17 this peak in the population will give rise to a corresponding peak in the emission spectrum with the outer turning point emitting a band near 265 nm and the inner turning point emitting somewhere to the red of 335 nm (as yet unobserved). As either temperature or density are raised, these high lying vibrational states are brought into thermal equilibrium with the lower states (which emit at 335 nm for example) thus the 265 nm band intensity decreases relative to the 335 nm band and it is not seen at all in thermal equilibrium (i.e.,  $n > 5 \times 10^{17} \text{ cm}^{-3}$  and  $T > 575 \text{ K}$ ; see Figs. 1, 2, 3, 4 and Sec. II of Ref. 1).

We have also seen the 254 nm band in absorption and our spectra agree with those seen by Kuhn<sup>24</sup> and by Perrin.<sup>25</sup> In particular the features designated I, II, III, and IV by Kuhn (see Fig. 5 of Ref. 24) are reproduced by our data shown in Fig. 18. We have analyzed the temperature dependence of the prominent peak and obtain a value for the ground state rotationless dissociation energy  $D_0$  of  $460 \text{ cm}^{-1}$ . This value is in close agreement with the value  $D_0 = 480 \text{ cm}^{-1}$  obtained by Frank and Grotrian<sup>26</sup> and by Koernicke.<sup>27</sup> It also agrees fairly well with the values  $530 \text{ cm}^{-1} < D_0 < 740 \text{ cm}^{-1}$  obtained by Kuhn and Freudenberg<sup>5</sup> and by Kuhn.<sup>24</sup> It differs quite markedly from the value  $974 \text{ cm}^{-1}$  obtained by Winans and Heitz<sup>28</sup> however these authors seem to have used the law of mass action incorrectly in their analysis.

It should also be mentioned that we attempted, without success, to directly pump the trimer with 351 nm  $(100 \text{ W/cm}^2)$  radiation in a cell at pressures up to 10 atm

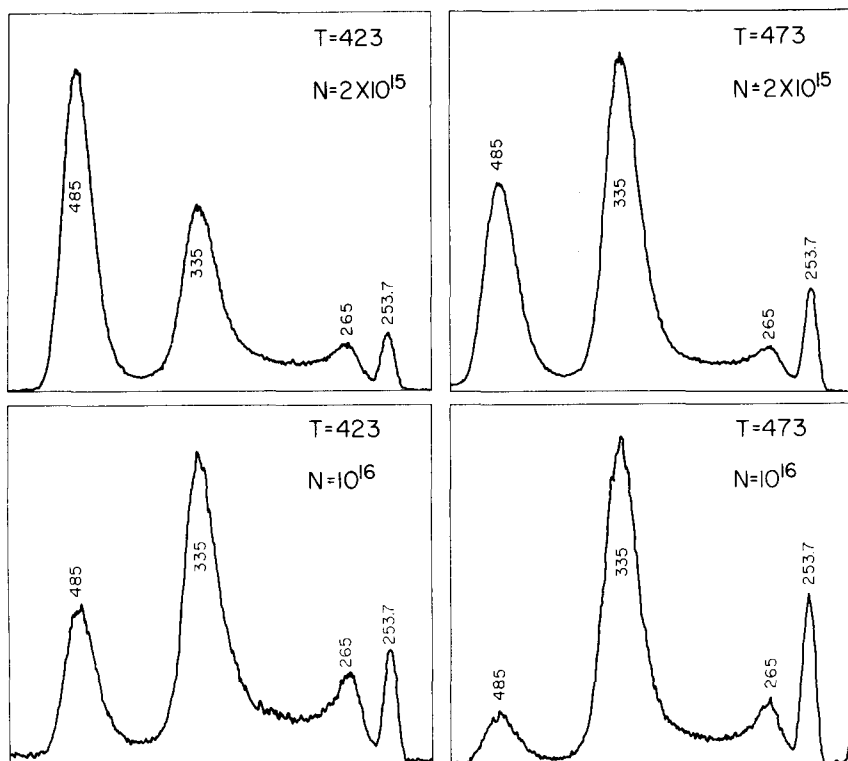


FIG. 16. Fluorescence spectra observed by Matland and McCoubrey<sup>23</sup> at two different temperatures and densities (in  $\text{cm}^{-3}$ ). Both the intensity and wavelength scales are uncalibrated, but the positions of the important emission features are noted. These spectra show an emission band at 265 nm which decreases relative to the 335 nm band when either temperature or density are increased. It is argued that this band is due to emission from a nonthermal population in the higher vibrational levels of the  $1_u$  state. This nonthermal population is created by excitation transfer from the  $6^3P_0$  metastable atomic state (see Fig. 17).

( $10^6$  Pa) and temperatures up to 1000 K. The ground state energy for this transition would be about  $1500 \text{ cm}^{-1}$ .

## VI. SUMMARY

We have studied the mercury excimer system under optical excitation and have shown the states responsible

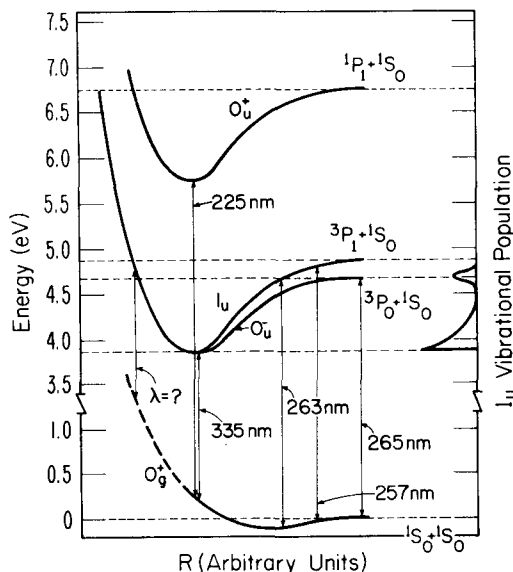


FIG. 17. Qualitative plot of the vibrational population in the  $1_u$  state (right hand ordinate axis) showing a thermal distribution in the lower lying states and a nonthermal population, fed by energy transfer from the  $3P_0$  atoms, in the higher states. This situation occurs for low densities and temperatures and is believed responsible for the emission feature seen at 265 nm (Fig. 16) as well as an emission to the red of 335 nm, which has not been observed as yet.

for the two prominent emission bands (335 and 485 nm) are in thermal equilibrium at gas densities greater than  $3 \times 10^{17} \text{ cm}^{-3}$  and gas temperatures greater than 575 K. We have made careful measurements of the shapes of these bands as a function of temperature, and this data is analyzed by Smith *et al.*<sup>1</sup> to obtain potential curves for the radiating states. The 335 nm radiator has been confirmed as a diatomic species through the pressure dependence of its absorption spectra. The 485 nm radiator has been shown to be a triatomic complex which lies some  $6500 \text{ cm}^{-1}$  below the state that radiates at 335 nm. The three body interaction responsible for the 485 nm radiation has been shown to be mercury specific. This observation supports the idea that the visible radiator is in fact a bound  $\text{Hg}_3$  triatomic excimer. Further evidence to support this assignment has come from a study of the kinetics of the mercury system<sup>22,29</sup> where the temperature dependent decay rate shows a thermal decomposition of the visible radiator.

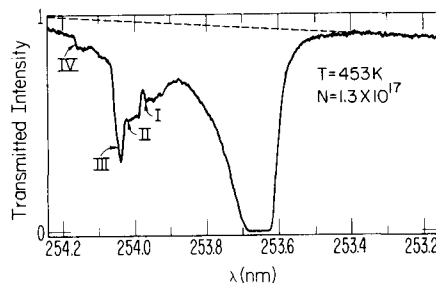


FIG. 18. Transmitted intensity with a 0.005 nm resolution and a 70.9 cm optical path at a density of  $1.3 \times 10^{17} \text{ cm}^{-3}$  and a temperature of 453 K showing the absorption features near 254 nm.

Absolute absorption measurements have been made in the 335 nm band to determine the oscillator strength of this transition and the ground state potential curve. Finally sequential or two photon excitation studies have been made which confirm the location of a metastable reservoir as well as the location of several higher lying excimer levels. These experiments, in conjunction with recent *ab initio* calculations<sup>21</sup> on Mg<sub>2</sub> were used to give the approximate location of some of the higher excited states of Hg<sub>2</sub>.

## APPENDIX

In Sec. IIIB it was noted that the molecular absorption measurements were occasionally complicated by the presence of atomic absorption lines arising from the <sup>3</sup>P<sub>0</sub> and <sup>3</sup>P<sub>1</sub> states. Even though the populations of these atomic states was very low, the atomic absorptions were excited exactly on line center because a mercury lamp was being used as a light source. The absorption was thus given by

$$\frac{d}{dx}I(\lambda, x) = -I(\lambda, x)[n^2k_m(\lambda) + n_a k_a(\lambda)] \quad (\text{A1})$$

where  $n_a$  represents the <sup>3</sup>P<sub>0</sub> and <sup>3</sup>P<sub>1</sub> atomic densities. Since the atomic states are excited by the molecular absorption,  $n_a$  is given by  $\tau I(\lambda, x)n^2k_m$  where  $\tau$  is a proportionality constant. This results in a nonlinear equation

$$\frac{d}{dx}I(\lambda, x) = -I(\lambda, x)[n^2k_m(\lambda) + \tau n^2I(\lambda, x)k_m(\lambda)k_a(\lambda)] \quad (\text{A2})$$

$$\approx -I(\lambda, x)[n^2k_m(\lambda) + \tau I_0 n^2k_m(\lambda)k_a(\lambda) \exp(-n^2k_m(\lambda)x)] ,$$

which was linearized by replacing the small nonlinearity by the zeroth order solution (i. e., the solution of the linear equation). The solution of this equation is

$$I(\lambda, x) = I_0(\lambda) \exp(-n^2k_m(\lambda)x - \tau I_0 k_a(\lambda) \{1 - \exp[-n^2k_m(\lambda)x]\}) . \quad (\text{A3})$$

At high densities the molecular absorption dominates (see Fig. 8) and one sees only  $n^2k_m(\lambda)$ . At low densities the absorption coefficient becomes

$$k(\lambda) \approx n^2k_m(\lambda) + \tau I_0 n^2k_m(\lambda)k_a(\lambda) . \quad (\text{A4})$$

The second term,  $\tau I_0 n^2k_m(\lambda)k_a(\lambda)$ , is actually proportional to  $n$  since the atomic absorption at line center is inversely proportional to the ground state atom density (e. g., a Lorentzian line profile is given by  $\gamma/(\Delta\nu^2 + \gamma^2)$  where  $\Delta\nu = (\nu - \nu_0)$  is the frequency separation from line center and the collisional line width  $\gamma$  is proportional to the atom density  $n$ ). This extra atomic absorption was found for all lines corresponding to transitions from the  $6^3P_0$  and  $6^3P_1$  states except for the measurements at 265 nm ( $6^3P_1-7D$ ) and 313.1 ( $6^3P_1-6^3D$ ) where the molecular absorption was so strong that it dominated the very weak atomic contribution. It is also interesting to note that an absorption measurement using a Cd line at 298 nm seemed to be absorbed off resonance by the mercury atomic transition  $6^3P_0-6^3D_1$  at 296.7 nm since an extra absorption coefficient proportional to  $n^3$  was

observed; note that off resonance the Lorentzian line profile is proportional to  $\gamma/\Delta\nu^2$  resulting in an  $n^3$  atomic term in Eq. (A4).

Using Eq. (A4) we could easily remove the effect of the atomic absorption and extract the molecular absorption coefficient from the experimental data. Unfortunately this method of analysis was not discovered until after the absorption measurements were completed and no measurements of the temperature dependence of  $k$  were made at those wavelengths where atomic absorption was present. This lack of temperature dependence prevents us from extracting an  $A$  value for these transitions [cf. Eq (3.2)].

\*Supported in part by ERDA Contract E(49-1)-3800 and by ARPA Order 891, Amendment 11.

<sup>1</sup>E. W. Smith, R. E. Drullinger, M. M. Hessel, and J. Cooper, *J. Chem. Phys.* **66**, 5667 (1977).

<sup>2</sup>R. W. Wood, *Physical Optics* (Dover, New York, 1961), p. 636.

<sup>3</sup>Lord Rayleigh, *Proc. R. Soc. London Ser. A* **114**, 620 (1927); **137**, 101 (1932).

<sup>4</sup>A. O. McCoubrey, *Phys. Rev.* **93**, 1249 (1954).

<sup>5</sup>H. Kuhn and K. Freudenberg, *Z. Phys.* **76**, 38 (1932).

<sup>6</sup>R. E. Drullinger, M. M. Hessel, and E. W. Smith, *Natl. Bur. Stand. (U.S.) Monogr.* **143** (1975).

<sup>7</sup>R. Lennuier and Y. Crenn, *C. R. Acad. Sci.* **216**, 486 (1943).

<sup>8</sup>J. Skonieczny and L. Krause, *Phys. Rev. A* **9**, 1612 (1974).

<sup>9</sup>A. G. Ladd, C. G. Freeman, M. J. McEwan, R. F. C. Claridge, and L. F. Phillips, *Trans. Faraday Soc.* **69**, 849 (1973).

<sup>10</sup>D. J. Eckstrom, R. M. Hill, D. C. Lorentz, and H. H. Nakano, *Chem. Phys. Lett.* **23**, 112 (1973).

<sup>11</sup>R. J. Carbone and M. M. Litvak, *J. Appl. Phys.* **39**, 2413 (1968).

<sup>12</sup>L. A. Schlie, B. D. Guenther, and D. L. Drummond, *Chem. Phys. Lett.* **34**, 258 (1975).

<sup>13</sup>H. Takeyama, *J. Sci. Hiroshima Univ.* **15**, 235 (1952).

<sup>14</sup>A. Atajew, A. Rutscher, and R. Winkler, *Beitr. Plasmaphys.* **12**, 239 (1972).

<sup>15</sup>E. R. Mosburg and M. Wilke, *J. Chem. Phys.* (to be published).

<sup>16</sup>P. Pringsheim, *Fluorescence and Phosphorescence* (Interscience, New York, 1949).

<sup>17</sup>A. C. Vikis and D. J. LeRoy, *Phys. Lett. A* **44**, 325 (1973).

<sup>18</sup>P. J. Hay, T. H. Dunning, and R. C. Raffanetti, *J. Chem. Phys.* **65**, 2679 (1976).

<sup>19</sup>R. Lennuier, *C. R. Acad. Sci.* **213**, 169 (1941).

<sup>20</sup>R. M. Hill, D. J. Eckstrom, D. C. Lorents, and H. H. Nakano, *Appl. Phys. Lett.* **23**, 373 (1973).

<sup>21</sup>W. J. Stevens and M. Krauss, *J. Chem. Phys.* (manuscript in preparation).

<sup>22</sup>M. Stock (unpublished data).

<sup>23</sup>C. G. Matland and A. O. McCoubrey (unpublished data).

<sup>24</sup>H. Kuhn, *Proc. R. Soc. London* **158**, 230 (1937).

<sup>25</sup>D. Perrin, Ph.D. thesis, University of Paris VI, 1974.

<sup>26</sup>J. Frank and W. Grotrian, *Z. Tech. Phys.* **3**, 194 (1922).

<sup>27</sup>E. Koerniecke, *Z. Phys.* **33**, 219 (1925).

<sup>28</sup>J. G. Winans and M. P. Heitz, *Z. Phys.* **133**, 291 (1952); **135**, 406 (1953).

<sup>29</sup>E. W. Smith (unpublished analysis).